Measurement of Wave-Induced Turbulent Flow Structures Using Digital Image Sequence Analysis

Dietmar Wierzimok [1] and Bernd Jähne [2]

doi: 10.5281/zenodo.12206

Abstract

The turbulent flow in water close to the wavy wind-stressed water surface has been examined quantitatively in a large circular wind-water tunnel with a flow visualization method using a special image sequence analysis. The flow field beneath the moving air-water interface is visualized by means of small polystyrol particles. These are illuminated by a thin light sheet, oriented along wind direction and parallel to the main flow field. The mie-scattered light of the particles is observed perpendicularly by a CCD video camera. First measurements, using two low cost image processing systems, allow a determination of velocity vectors in image sequences of up to 32 binary images. The tracking algorithm solves the correspondence problem of a particle's path in subsequent images by use of the particle's orientation and the video interlaced mode. Since every particle is traced along its full path within the light sheet, both the Eulerian and the Lagrangian velocity fields can be calculated. This provides access of a new kind to the examination of transport and turbulence below the surface, as demonstrated by means of different evaluation methods for the calculation of spatially dependent velocity distributions, the Stokes drift and friction velocity.

Introduction

The interplay between the wind-wave driven turbulent flow structure close to a free water surface and molecular diffusion determines the gas exchange rate between atmosphere and oceans (Jähne et al. 1987). Direct measurements of the turbulence from about one meter depth up to the mass boundary layer are one key to increase knowledge about gas transfer. In conjunction with wave measurements, this is the right tool to investigate the influence of waves on the gas exchange process – one of the most demanding theoretical problems. The method is especially useful in order to examine the turbulent patches generated by breaking waves and their influence on the gas exchange process.

Unfortunately, flow measurements close to a moving interface are technically very difficult. Basically, two approaches exist. First, laser doppler anemometry (LDA) can be applied where the measuring position follows the water surface with an optical scanner. This technique has been used successfully by (Cheung and Street 1988) with regular mechanical waves. Its disadvantage is that no spatial data are gained which are essential to measure the spatial and temporal scales of turbulent patches.

In order to obtain spatial velocity data, flow visualization represents an alternative method to measure the turbulent flow close to the water surface (Hesselink 1988). Although a lot of experimental information can be gained by using this method (e.g. the papers of Okuda (Okuda 1982, Okuda et al. 1976) and (Nadaoka et al. 1989), the quantitative evaluation of the images involves an enormous amount of work.

[1]Institut für Umweltphysik (IUP) and Interdisziplinäres Zentrum für wissenschaftliches Rechnen (IWR), Universität Heidelberg, Im Neuenheimer Feld 366, D-6900 Heidelberg, West Germany

[2]Scripps Institution of Oceanography A-030, La Jolla, CA 92093, USA

Reprinted from Air-Water Mass Transfer
Second International Symposium
U.S. Army Waterways Experiment Station/ASCE
Minneapolis, MN, Sept. 11-14, 1990

This paper combines classical flow visualization techniques and particle tracking with modern digital image sequence processing techniques. The new experimental tool allows the analysis of the Eulerian as well as the Lagrangian flow field, with the developed particle tracking algorithm running over long image sequences.

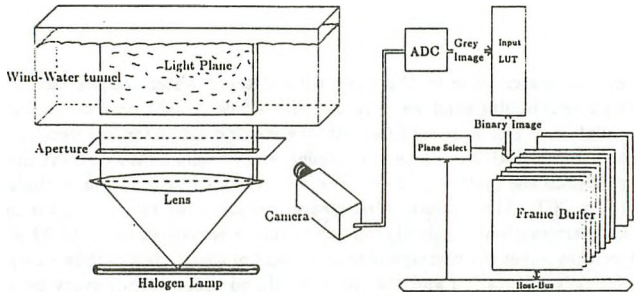

Fig. 1: Arrangement of the wind-water tunnel, the optical system, the camera and the image processing system. From (Wierzimok and Jähne 1989).

Experimental Set-Up

The experiments have been performed at a water depth of 30 cm in the large circular wind-water tunnel at Heidelberg (r_T=2 m, width=30 cm), where wind speeds of up to 10 m/s are generated by a rotating PVC ring 30 cm above the water surface.

The turbulent flow has been visualized using spherical polystryrol particles with diameters ranging from 50 to 150 μm. Since their density is close to the density of water (1.04 g/cm^3) they show good tracking behavior and only small buoyancy effects (Agüí and Jiménez 1987). The visualization error is the error in velocity caused by the tracking delay between particles and fluid. It depends on the particles size and density and the fluctuation of the fluid velocity (Hjelmfelt and Mockros 1965) and has been pointed out to be equal less than 0.1% (Wierzimok 90) for the observed flow fields.

The particles are illuminated from below by a thin vertical along-wind oriented light sheet of 1.5 cm to 3 cm thickness. The sheet is generated by a halogen lamp with an asymmetric plano-convex and a fresnel lens. The image sequences are taken with a CCD-video camera, whose optical axis is oriented perpendicularly to the illuminated plane (fig. 1). The video data are digitized and stored as binary images in the frame buffer of a PC-based image processing system with a spatial resolution of 512^2 pixels (using ITI FG-100 and Matrox MVP-AT boards).

Image Sequence Processing

The image processing algorithm mainly consists of four steps: the real time object segmentation, the particle segmentation, the particle tracking and the transformation from image to world coordinates. The first two steps include the low level image preprocessing in order to separate the particles from the background and to determine the water surface. The third step analyzes the velocity of every detected particle in the image sequence along its projected path in image coordinates, which are transformed to planar world coordinates in the last image processing step.

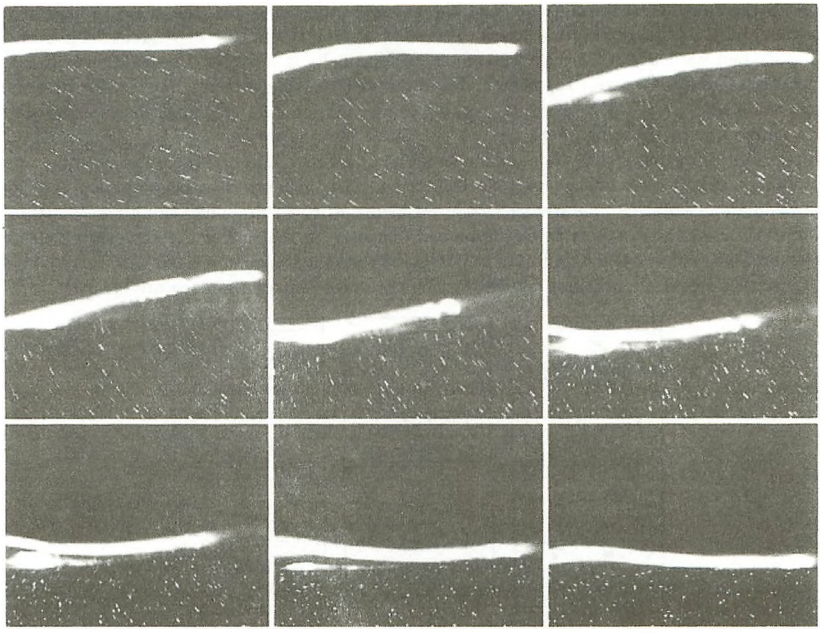

Fig. 2: A digitized sequence consisting of 9 consecutive images of a 13 cm (horizontal) × 9 cm (vertical) observed area at a wind speed of 9 m/s. The bright area at the upper part represents the water surface.

Real time segmentation

Due to the enormous rate of image data produced by the video camera (6 MByte/s in Europe) and the limited capacity of the frame memory, a real time data reduction has to be implemented in order to keep a long image sequence digitized in the frame buffer accessible for further processing (what long enough means will be discussed later). Here real time refers to a sufficiently fast procedure capable of reducing every single video image entirely during the exposure time of the next one - 40 ms in Europe (1/25 Hz) and 33 ms in the USA (1/30 Hz). This has been realized by means of the Input Look-up-table (INLUT) of the frame grabber's hardware which allows a programmed conversion of every pixel incoming from the camera in dependence of its grey value. Mathematically this corresponds to a homogeneous point operation. With a global grey value threshold, adapted manually to separate background and particles (segmentation), the one byte information of every grey value from zero to 255 is reduced to a binary value with only one bit per pixel where zero refers to the background and one refers to the object (fig. 2). Thus, not only 4 grey value images, but a whole sequence of up to 32 consecutive binary images can be recorded and stored in the 1 Mbyte frame buffer in real time.

Water surface-particle segmentation

Due to the continuous illumination and the exposure time of 40 ms, the binary image sequence contains particle traces as thin streak lines with a typical velocity dependent length of about 20 pixels and with about 2.5 pixels diameter. Additionally, a horizontal wavy line with a typical diameter of about 80 pixels represents the water surface. The surface line has to be separated from the streak lines before particle tracking can be carried out. This has been achieved by use of a morphological *opening* operation – a non-linear filtering process (see i.e. Zamperoni 1990 or Serra 1982) – for every single binary image (Wierzimok and Jähne 1989). The *opening* operator eliminates 'small' objects (the particle traces) and the thick surface line remains, allowing the approximate calculation of water surface levels by means of a simple line thinning algorithm. The maximum size of the objects to be eliminated, depends on the size of the structuring element of the morphological operation and may be compared to the hole size in a sieve. An image containing only particle streaks is obtained by subtracting the *opened* image from the original one.

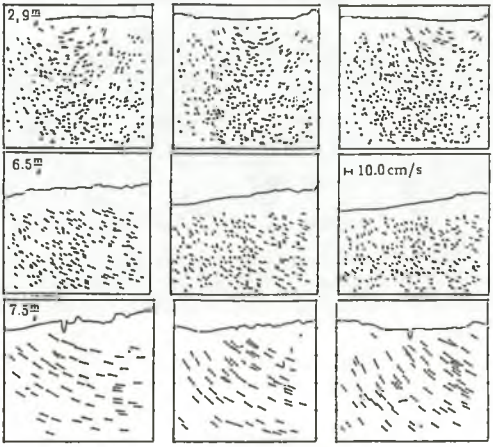

Fig. 3: Measured vectors of three consecutive images at the wind speeds 2.9, 6.5 and 7.5 m/s. The origins are marked by a small dot. The window size is the same than in figure 2.

Particle Tracking

The main step, the particle tracking algorithm, automatically traces a particle's path from image to image through the complete sequence. As a result, a chain of two–dimensional displacement vectors $\mathbf{u}_j(t_0 + iT)$ is obtained for every particle j, where i denotes the image number and T denotes the reciprocal video image frequency ($T = 20$ ms in Europe).
The algorithm uses physical as well as heuristic concepts. The basic idea is to make use of the special pattern of moving objects in every single image as a consequence of the video signal characteristic. The interlaced mode of the video camera causes the exposure time T of a single image to separate into two different intervals for the odd and the even lines of a frame. For the camera used, these

are consecutive intervals each lasting about $T/2$, so that a moving object first appears in the odd, then in even lines of a single full image. Consequently, all moving particles appear as interleaved patterns which allows an easy discrimination of resting objects. Instead of using the line ends of a detected and segmented particle's streak, the centers of mass of object pixels (value one) in odd and even lines are used to detect movement. Their displacement $s_{j,i}$ includes both orientation as well as direction of the particle belonging to the streak line. The estimated position of the corresponding streak line of the same particle in the next frame (i+1) can be estimated easily from its displacement vector within the single image (i), so that no time costly cross correlation has to be carried out in order to solve the correspondence problem.

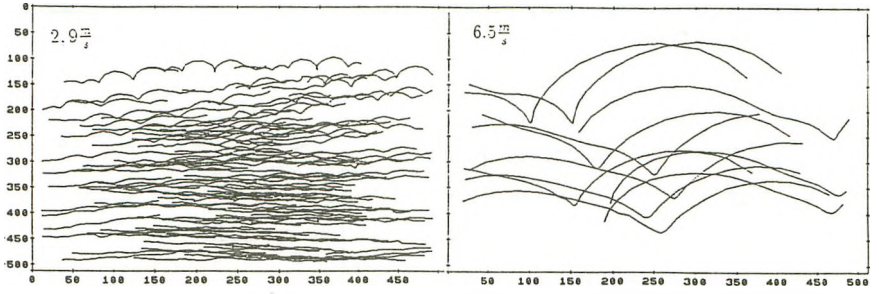

Fig. 4: Particle trajectories at 2.9 and 6.5 m/s wind speed (axis in pixels). Only trajectories of particles, that have been tracked longer than 1 s are presented.

Additional physical constraints are included in order to avoid faulty correspondences. The accepted amount of absolute velocity $u_{j,i}$ and acceleration $a_{j,i}$ between two consecutive images

$$u_{j,i} = \frac{s_{j,i}}{T/2} \tag{1}$$

$$a_{j,i} = \frac{u_{j,i+1} - u_{j,i}}{T} \tag{2}$$

during a particle's path within the observed light sheet is restrained to a maximum of $u_{max} = 40\,\mathrm{cm/s}$ (80 pixel/image) and $a_{max} = 3\,\mathrm{m/s^2}$, which is calculated from the physically attempted limits of the orbital movement. The accuracy of the correspondence has been examined by a manual control and been estimated to equal 95% approximately.

Transformation

In order to allow transformation from image to world coordinates, the coefficients of the transformation matrix are estimated using a grid (mesh width 0.5 cm) positioned in the center light sheet for spatial calibration. Neglecting the depth of the light sheet, the transformation of the world coordinates $P(x, y)$ (9 cm × 13.5 cm) to the image coordinates $P(x', y')$ (512 × 512 pixels) can be described as a central projection from one plane onto another as follows

$$x' = \frac{a_1 x + a_2 y + a_3}{c_1 x + c_2 y + 1} \quad \text{and} \quad y' = \frac{b_1 x + b_2 y + b_3}{c_1 x + c_2 y + 1}$$

The equations for the pass points P_i ($i > 4$) correspond to an overdetermined set of $2i$ linear equations is given for the eight projection parameters $a_1 \cdots c_2$. This has been solved with standard

techniques as described i.e. in (Teukolsky 1988). An accuracy of about 0.25% in both directions was achieved (Wierzimok and Jähne 1989).
Additionally, the systematic velocity error produced by a particle's distance z from the calibrated focus plane (out-of-plane motion) can be estimated by

$$\frac{\Delta u}{u} = \frac{z}{d} \quad , \tag{3}$$

if z doesn't change during the particles motion between two images ($u_z = 0$). This means that the flow field is considered two-dimensional. The fraction-corrected distance between camera and focus plane is denoted by d (here $\approx$ 57,6 cm). The maximum error in the present case, where, due to the binary threshold the efficient thickness of the light plane is reduced, has been estimated to equal approximately 0.5% of the particles velocity.

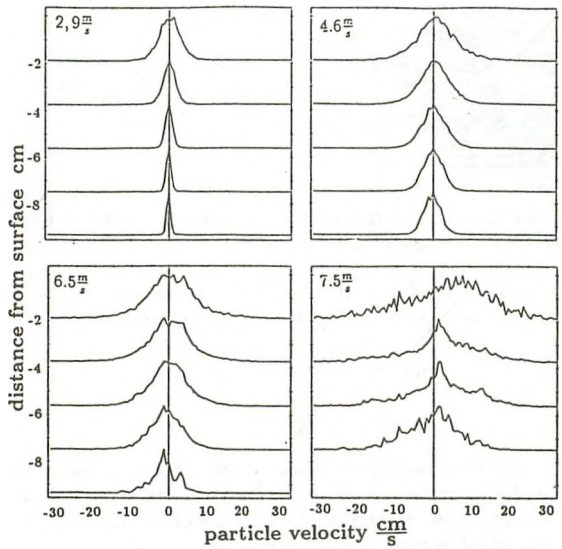

Fig. 5: Presentation of the velocity distribution at four different wind speeds (2.9, 4.6, 6.5, 7.5 m/s) and at different distances from the mean water surface position using ensembles of sequences at the same wind speed.

Results

The streak lines represent the time integrated particles' movement. The use of the pixels' center of mass for the displacement detection allows the subpixel calculation of the corresponding particle's mean position during exposure time. The subpixel accuracy has been estimated for the binary images at about 0.2 pixels by means of an integrated shifting Gaussian signal as a model for the

particle's movement during the exposure interval (Wierzimok 90). Thus, with the imaging window used (9 cm height and 13 cm width) the maximum error for the velocity value equals about 3 mm/sec for binary images.

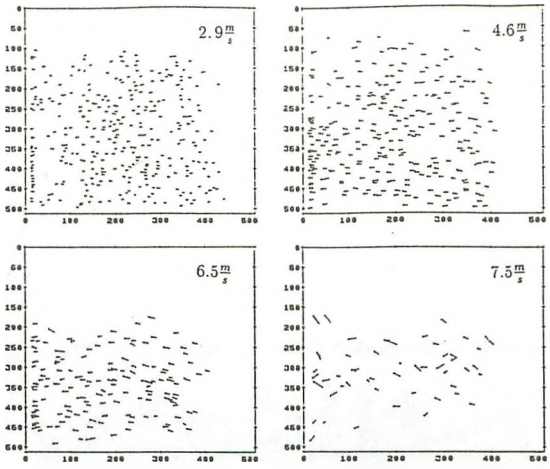

Fig. 6: Vector presentation of the mean Lagrangian drift velocity at different wind speeds of particles with 0.64 s minimum visibility.

Due to the tracking algorithm, the velocity vectors are available in the Lagrangian as well as the Eulerian specification. A typical sequence has a duration of 1.3 seconds (32 images), includes 5000 up to 15000 vectors of some 100 up to 500 recognized particles, and requires a total computing time of about 4 to 8 minutes on a PC-AT-386 computer without using any special hardware operation feature of the MVP image system. Up to 430 particles per 512x512 pixel image area have been detected and evaluated. Depending on the particles' velocities, up to 12 particles within an area of one square centimeter may be resolved.

Measurements of the two-dimensional velocity vectors at wind speeds ranging from 2.9 to 7.5 m/s with maximum wave amplitudes of up to 6 cm (trough to crest) reveal the advantages of area extended techniques. In order to demonstrate the far-reaching possibilities of the new technique, the obtained particle velocities from a series of first measurements have been evaluated in different ways. Figure 3 shows the measured Eulerian velocity vectors within three consecutive images at 2.9 and 7.5 m/s wind speed. This presentation provides spatial information about the flow structure and their temporal development. A better visualization of the orbital movement may be achieved using the particle's trajectory within the illuminated volume (fig. 4).

From the distribution of the vertical velocity component at different surface distances (fig. 5) the penetration depth of the dominant surface wave can be calculated from the decrease of the velocity variance assuming that this is mainly an effect of the orbital movement. In the distribution of a single sequence a certain amount of skewness has been observed which disappears when the complete ensemble of all sequences measured at the same wind speed is being used instead. The result is a zero mean value of the vertical velocity component, which reveals that the orbital

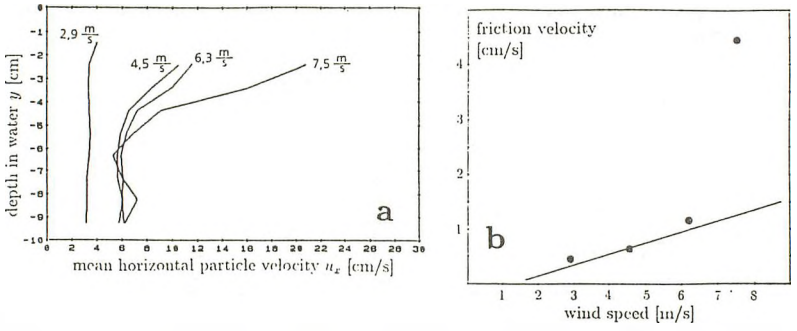

Fig. 7: The measured velocity profile (a) and the friction velocity u_* as a function of wind speed (b). u_* is calculated from the measured particle velocities as $\sqrt{-\overline{u_x u_y}}$. The line represents the calculated u_* from earlier measurements by a swing method (Bösinger 1985).

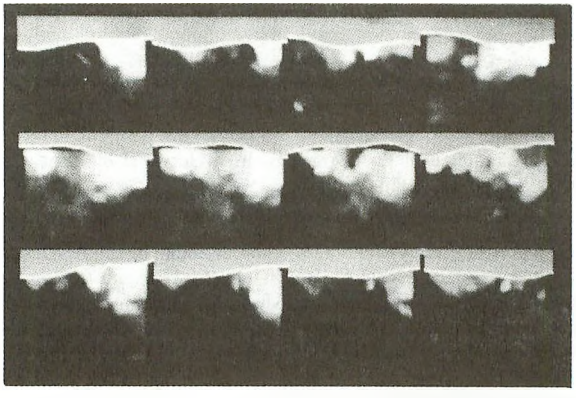

Fig. 8: Interpolation of the kinetic energy (u^2) within 12 subsequent images (13x9 cm) at 4.5 m/s wind speed. A high grey value below surface corresponds to a high energy value.

movement is compensated by use of long sequences or an ensemble of sequences and that only isotropic turbulence, if any, may be observed. For 7.5 m/s wind speed, however, the distribution seems to look different. The increasing wind speed causes dominant gravity surface waves with longer wavelengths and lower frequencies (about 1 m with 0.5 Hz at 7.5 m/s). For a zero mean value compensation of the orbital movement, the length of the observed sequence (or the sum of all sequences belonging to the same ensemble) has to be a multiple of the longest wave period. In case of the 7.5 m/s wind speed a multiple of 2 seconds (50 images) would be necessary. Due to the technical confinement during this first measurement campaign this condition is not fulfilled, thus leading to the non zero mean values of the vertical velocity distribution. Looking at the calculated mass transport expressed by the Lagrangian mean velocity (Stokes drift) and the turbulent friction velocity (fig. 6 and 7), especially this problem has to be taken into account at the highest wind speed.

Finally, the calculation of the kinetic energy of the flow turns out to be a good indicator for turbulent

patches produced by instabilities of the surface waves (fig. 8). An interpolation technique is used to calculate a continuous velocity field. The spatial resolution thereby is approximately equal to the mean distance of the particles (Agüí and Jiménez 1987). The curl of this vector field also highlights turbulent regions in the flow.

Conclusions

The first results are encouraging and prove that a new experimental tool is available which will be used in the near future for systematic studies of the turbulent water flow close to the water surface in different wind-wave facilities.

Further technical improvements are envisaged. The accuracy of the velocity determination can be improved significantly by using a smaller window size and by the use of image processing hardware that allows the recording of long grey value instead of only binary image sequences. In addition, the parallel nature of the observed particle movement longs for a parallel program design that will be developed on a supercomputer (supercluster-transputersystem at the IWR, Heidelberg). Yet, it seems to be most important to extend the technique from 2D- to 3D-velocity measurements. One promising proposition is the use of stereo images using the complete particles' path for stereo correlation.

Appendix. Notation

$a_{j,i}$	=	acceleration of particle j between image i and $i+1$
a_{max}	=	maximal accepted particle acceleration
$2s_{j,i}$	=	displacement vector of particle j in image i
T	=	exposure time of a full image
P_i	=	pass point in world and image coordinates
r_T	=	Outer radius of the circular wind-water tunnel in Heidelberg
u_x	=	horizontal velocity component
u_y	=	vertical velocity component
$u_{j,i}$	=	velocity vector of particle j in image i
u_{max}	=	maximal accepted particle velocity
x',y'	=	horizontal and vertical position in image
x,y,z	=	world coordinates

Appendix. References

Agüí, J.C., Jiménez, J., 1987, 'On the performance of particle tracking', *Journal of Fluid Mechanics*, 185, 447–468.

Bösinger, R., 1986, 'Messungen zur Schmidtzahlabhängigkeit des Gasaustausches', *Diplomarbeit, Institut für Umweltphysik*, D–221, Universität Heidelberg

Cheung, T. K., R. L. Street, 1988, 'Wave-following measurements in the water beneath an air-water interface', *J. of Geophysical Research*, 93, p.14089–14097.

Hesselink, Lambertus, 1988, 'Digital image processing in flow visualization'. *Ann. Rev. Fluid Mech.*, 20, 421–485.

Hjelmfelt,A.T., L.F. Mockros, 1965, 'Motion of Discrete Particles in a Turbulent Fluid', *Appl. Sci. Res.*, 16, 149–161

Jähne, B., K.O.Münnich, R.Bösinger, A.Dutzi, W. Huber, P. Libner, 1987, 'On the parameters influencing air-water gas exchange', *J. Geoph. Res.*, 92, pp. 1937–1949

Jähne, B., 1990, *Digitale Bildverarbeitung*, Springer-Verlag, Heidelberg

Nadaoka, K., M. Hino, Y. Koyano, 1989, 'Structure of the turbulent flow field under breaking waves in the surf zone', *Journal of Fluid Mechanics*, 204, 359–387.

Okuda, K., S.Kawai, M.Tokuda, Y. Toba, 1976, 'Detailed observation of the wind-surface flow by use of flow visualization methods', *J. of the Oceanographical Society of Japan*, 32, 53-64

Okuda, K., 1982, 'Internal flow structure of short wind waves, Part I. On the internal vorticity structure', *J. Oceanogr. Soc. Japan*, 38, p.28–42.

Okuda, K., 1982, 'Internal flow structure of short wind waves, Part II. The streamline patterns' *J. Oceanogr. Soc. Japan*, 38, p.313–322.

Serra, J., 1982, *Image analysis and mathematical morphology*, Academic Press London

Teukolsky, S. A., W. T. Vetterling, 1988, *Numerical recipes, the art of scientific computing*, Cambridge University Press

Wierzimok, D, B. Jähne, und J. Dengler, 1987, 'Bildfolgenanalyse dreidimensionaler turbulenter Strömungen', *Proc. 9.DAGM-Symp. Mustererkennung 1987, Informatik-Fachberichte*, 149, Springer-Verlag, Berlin

Wierzimok, D., Jähne, B., 1989, '3-dimensional particle tracking beneath a wind-stressed wavy water surface with image processing', *Proc. 5th Int. Symp. Flow Visualization*, Prag 1989 (in press)

Wierzimok, D., 1990, 'Messung turbulenter Strömungen unterhalb der wind-wellenbewegten Wasseroberfläche mittels Bildfolgenanalyse', *Dissertation. Universität Heidelberg*, Fakultät Physik

Zamperoni, P., 1989 *Methoden der digitalen Bildverarbeitung*, Vieweg, Braunschweig